Theory of Strain Relaxation in Epitaxial Growth

A. C. Schindler[1], M. F. Gyure[2], G. D. Simms[2], D. D. Vvedensky[1], R. E. Caflisch[3], C. Connell[4] and E. Luo[3]

[1] The Blackett Laboratory, Imperial College, London

[2] HRL Labs

[3] Department of Mathematics, UCLA
Los Angeles, CA

[4] Department of Mathematical Sciences and
Center for Applied Mathematics and Statistics
New Jersey Institute of Technology, Newark, NJ 07102

CAMS Report 0203-18, Spring 2003

Center for Applied Mathematics and Statistics

NJIT

Theory of Strain Relaxation in Heteroepitaxial Systems

A. C. Schindler[1], M.F. Gyure[1,2], G. D. Simms[2], D.D. Vvedensky[1], R. E. Caflisch[3,4], C. Connell[3] and Erding Luo[3]

[1] *The Blackett Laboratory, Imperial College, London SW7 2BZ, United Kingdom*

[2] *HRL Laboratories LLC, 3011 Malibu Canyon Road, Malibu, CA 90265*

[3] *Department of Mathematics, University of California, Los Angeles, CA 90095-1555*

[4] *California NanoSystems Institute and Department of Materials Science & Engineering, UCLA.*

(Dated: July 15, 2002)

We introduce a general approach to calculating the morphological consequences of coherent strain relaxation in heteroepitaxial thin films based on lattice statics using linear elasticity. The substrate and film are described by a simple cubic lattice of atoms with localized interactions. The boundary conditions at concave and convex corners that appear as a result of this construction, those along straight interfacial segments, and the governing equations are obtained from a variational calculation applied to a discretized form of the total elastic energy. The continuum limit of the equations and the boundary conditions along straight boundaries reproduces standard results of elasticity theory, but the boundary conditions at corners have no such analogue. Our method enables us to calculate quantities such as the local strain energy density for any surface morphology once the lattice misfit and the elastic constants of the constituent materials are specified. The methodology is illustrated by examining the strain, displacement and energies of one-dimensional strained vicinal surfaces. We discuss the effects of epilayer thickness on the energy of various step configurations and suggest that coupling between surface and substrate steps should affect the equilibration of the surface toward the bunched state.

PACS numbers: 68.55.-a, 68.35.Gy, 68.60.-p

I. INTRODUCTION

The structural and compositional integrity of heteroepitaxial films is central to the fabrication of all quantum heterostructures. The morphology of these films is determined by

a number of factors, including the manner in which strain is accommodated if the materials have different lattice constants, the surface and interface energies of the materials, and any effects associated with alloying and segregation. Thermodynamic arguments based on interfacial free energies are often used to provide a classification scheme for the *equilibrium* morphology of thin films[1]. But while such considerations undoubtedly play an important role in providing the overall driving force for the morphological evolution of thin films, they neglect a number of inherently kinetic effects. The interplay between thermodynamics and kinetics is especially germane to heteroepitaxial systems where, for example, variations in growth conditions (substrate temperature, flux, substrate misorientation) and annealing are used to manipulate the spatial and size distributions of three-dimensional (3D) coherent islands that appear during the Stranski–Krastanov growth of lattice mismatched semiconductors for quantum dot applications[2].

Strain relaxation in heteroepitaxial systems has been the subject of an abundance of theoretical studies, but there is yet no general methodology with the versatility of the Burton–Cabrera–Frank theory[3], rate equations[4], or kinetic Monte Carlo simulations[5] which captures the essence of thin film evolution in the presence of lattice misfit. There are two main reasons for this. The rates of atomistic processes on strained surfaces are not determined solely by the local environment of the atoms, as in the case of homoepitaxy, but may depend on nonlocal features such as the *height* of a terrace above the initial substrate, the *size* and *shape* of two- and three-dimensional islands[6,7], and their local environment[8]. This is further complicated by the competition between different strain relaxation mechanisms (e.g., alloying, misfit dislocation formation, surface profile modulations), each of which has a characteristic signature in the morphology of the substrate[9]. Additionally, any general theoretical approach must incorporate long-range elastic interactions, which are best treated within a continuum framework, and atomistic effects such as step-adatom interactions, alloying and possibly reconstruction changes during growth.

The theoretical description of the formation of heterogeneous interfaces falls into one of three broad categories: (i) the minimization of energy functionals, including thermodynamic potentials, of various levels of sophistication to determine *equilibrium* atomic positions as a function of the lattice mismatch[6,10,11], (ii) kinetic Monte Carlo simulations, both lattice-based[7,12] and off-lattice[13], where the hopping rules are modified to account for the effects of strain on diffusion and adatom attachment and detachment at step edges, and (iii) classical

elasticity theory applied to the evolution of the growth front profile of continuous films[14,15]. These studies all require a compromise between a realistic description of interatomic interactions and the mesoscopic effects of strain relaxation due to lattice misfit.

The approach we describe in this paper is based on classical elasticity, but with the substrate and film composed of an atomistic grid, as in the method of lattice statics[16,17,18]. The lattice mismatch and the difference in elastic constants between the film and the substrate enter explicitly into this theory. This representation of the growing film is capable of including both atomistic and continuum elastic aspects of morphological energetics and kinetics. At the atomistic level, this includes the effect of strain on adatom diffusion[19], and the kinetic[6,7] and thermodynamic[10,20,21] stability of islands. Over larger length scales, there are interactions due to substrate distortion, which lead to a repulsive interaction between islands[10,22] and other surface species[23,24]. While such long-range effects are directly amenable to a description within continuum elasticity with suitably-chosen materials parameters, more localized effects can be modeled with empirical or first-principles methods, especially where a direct connection between the atomistic and continuum formulations can be established[25]. Our approach can be made consistent with atomistic models cast in a valence force field representation. This allows us the flexibility to, if desired, incorporate atomistic effects where needed while remaining within the general framework of linear continuum elasticity.

In this paper, we formulate the elasticity equations and boundary conditions for discrete substrates and films. In contrast to the situation for continuous films, where the boundaries are smooth curves[14], the boundaries of our discrete systems are piecewise constant, and this requires a separate treatment. Accordingly, we derive the elasticity equations and boundary conditions from a variational calculation applied to the total elastic energy of a discretized system which respects the local symmetries of all points. The equations obtained for the interior region and along straight segments of the boundary lead, in the continuum limit, to the usual equations and boundary conditions, respectively, of linear elasticity. But at corners, the boundary conditions are best understood in quasi-atomistic terms as a constraint on the local displacement. We illustrate our method by calculating the interactions between steps on one-dimensional strained vicinal surfaces, which is relevant to the step-bunching instability on such surfaces. We examine qualitatively and quantitatively the strain and displacement fields that arise from the model and compare and contrast these results to known results from continuum elasticity. We also examine the influence of the thickness of

the epilayer and the differences in the elastic properties between the film and the substrate and discuss the implications of these on the evolution toward the bunched state.

The outline of this paper is as follows. The basic equations of linear elasticity are reviewed briefly in Sec. II. The details of our model are then presented in Sec. III where we describe our variational formulation of the discretized equations and boundary conditions. The complete set of equations describing the boundary conditions are compiled in the Appendices. In Sec. IV we describe some results of our model including a comparison between step–step interactions in continuum elasticity and those calculated within our model. We also present results obtained from the application of our model to vicinal surfaces that are relevant to the step-bunching instability on a one-dimensional strained vicinal surface. In particular, we discuss the likely influence of epilayer thickness and lattice mismatch of the substrate and epilayer on the evolution of the film toward the bunched state. Finally, in Sec. V we summarize our results and outline future applications of our approach.

II. CLASSICAL ELASTICITY

The following discussion presumes that the system is two-dimensional (i.e., that the substrate is one-dimensional), but the extension to a 3D system (i.e., a two-dimensional substrate) is straightforward. Let u_k, where $k = 1, 2$, denote the Cartesian components of the displacement vector. For linear elasticity in an isotropic material, the components of the strain tensor S and stress tensor T are given in terms of the displacement vector by[26]

$$S_{k\ell} = \tfrac{1}{2}\left(\partial_k u_\ell + \partial_\ell u_k\right) \tag{1}$$

$$T_{k\ell} = \lambda \delta_{k\ell} S_{nn} + 2\mu S_{k\ell}, \tag{2}$$

where $\partial_1 \equiv \partial/\partial x, \partial_2 \equiv \partial/\partial y$ and λ, μ are the Lamé constants. Repeated indices imply summation from 1 to 2. For the heteroepitaxial growth of a film with lattice constant a_f on a substrate with a lattice constant a_s, the normalized lattice mismatch is

$$\epsilon = \frac{a_f - a_s}{a_s}, \tag{3}$$

The strain tensor for the film is given by

$$S'_{k\ell} = \tfrac{1}{2}\left(\partial_\ell u'_k + \partial_k u'_\ell\right), \tag{4}$$

where the prime denotes quantities associated with the film. Using Eq. (3), S' can be expressed in terms of displacements with respect to the substrate lattice positions as

$$S'_{k\ell} = S_{k\ell} + \delta_{k\ell}\epsilon, \tag{5}$$

Accordingly, the corresponding stress tensor T' for the film is

$$T'_{k\ell} = \lambda'\delta_{k\ell}S_{nn} + \mu' S_{k\ell} - (2\lambda' + \mu')\,\delta_{k\ell}\epsilon. \tag{6}$$

In mechanical equilibrium the forces inside any volume Ω vanish,

$$\nabla \cdot T = 0, \tag{7}$$

and the force on the boundary $\partial\,\Omega$ equals the external pressure (in the absence of external tractions which in the case of vacuum is zero), leading to

$$\mathbf{n} \cdot T = 0 \quad , \tag{8}$$

where $\mathbf{n} = (n_1, n_2)$ is the vector normal to the surface. Additionally, at the interface between the film and the substrate, the normal component of the stress is continuous:

$$\mathbf{n} \cdot T = \mathbf{n} \cdot T' \quad . \tag{9}$$

For a continuous film, Eqs. (7), (8), and (9) completely specify the distribution of stress within the system. For the purpose of the discussion in the next section, it is useful to point out here that the above boundary conditions can be derived from a variational principle applied to the total elastic energy. The elastic energy density $\mathcal{E}$ of the strained substrate is given by the tensor contraction $\frac{1}{2}S : T$. In terms of Cartesian components,

$$\begin{aligned} \mathcal{E} &= \tfrac{1}{2}S : T \\ &= \tfrac{1}{2}\lambda\left(\partial_n u_n\right)^2 + \tfrac{1}{2}\mu\left[\left(\partial_k u_\ell\right)^2 + \partial_\ell u_k \partial_k u_\ell\right] \end{aligned} \tag{10}$$

so that the total elastic energy is

$$E_{\mathrm{E}} = \int_\Omega \mathcal{E}\; dx. \tag{11}$$

The force balance equations and boundary conditions for each point then follow from setting the variation of the elastic energy with each of the displacements equal to zero:

$$\frac{\delta E_{\mathrm{E}}}{\delta u_{k\ell}} = 0, \tag{12}$$

where $u_{k\ell} = \partial_\ell u_k$.

III. MODEL

In this section we will describe a discrete atomistic model for strain, designed to agree with continuum elasticity in those regions where continuum theory has a natural discretization (namely in the bulk and at straight boundaries).

A. Elastic boundary conditions for discrete films

For our system, we have used an approach to formulating the equations of elasticity, based on lattice statics, that is especially appropriate for epitaxial systems. This methodology is explained in detail in[27]. Here we outline the general structure of the method; mathematical details are included in the appendices. The general approach is to not discretize the equations (12) directly. Instead, we construct a discrete version of the elastic energy density (10), and then define the total energy as a sum of this energy density over lattice points:

$$E_{\mathrm{T}} = \Sigma_{i,j}\mathcal{E}(i,j) \tag{13}$$

At each point (i, j) of the grid, the energy contribution $\mathcal{E}(i, j)$ only involves terms from the 9 point stencil (nearest and next-nearest neighbors) centered at (i, j). The energy contribution per site $\mathcal{E}(i, j)$ is written in its most general form in Appendix A, and specific cases of interest are described in Appendices A and B.

The principal virtue of this formulation is that it combines atomistic and continuum approaches. If the computational grid is the same as the underlying atomistic lattice, then the discrete version of the energy may be considered purely atomistic. This correspondence is equivalent to imposition of the Cauchy-Born hypothesis, that the atomistic lattice displacement equals the macroscopic elastic displacement. The advantage of the atomistic interpretation is that it allows us to tailor the energy density to suit specific atomistic geometries where continuum elasticity fails to inform us as to what discrete equations to use. In particular, we have used it here to derive numerical boundary conditions at the sharp corners at the top of the film, and to derive equations at the film/substrate interface.

Using the discrete version of Eq. (10), the discretized force balance laws come from minimizing the total energy E_{T}. The resulting equations are

$$\frac{\partial E_{\mathrm{T}}}{\partial u_k(i,j)} = 0 \tag{14}$$

which is the discrete analogue of (12). These discrete equations are formally equivalent to discretizations of the classical elasticity equations. In particular, at interior points Eq. (14) is a discretization of Eq. (7), and at flat edges it is a discretization of Eq. (8). At corners and at material interfaces, however, these equations are new and do not admit a continuum interpretation.

The boundary conditions that arise from performing a variation on the discrete energy have the effect of regularizing the singularities that exist at, e.g., interior corner points. This regularization is not completely artificial; since our discretization is at the atomic scale, it is performed at the appropriate length scale. In a real material, the singularities present in continuum elasticity are, in fact, regularized by the atomic lattice. This regularization could be done in a more controlled fashion, entirely within our framework, by using an appropriately parameterized atomistic bond model for the energy at these singular points. This is beyond the scope of the present work, however, and we expect that qualitatively correct results for step equilibrium and dynamics can be obtained with the present form of the energy.

Our method for treating elasticity should be placed in context with an alternative approach[29,30], which is based on the use of Green's functions. This approach makes use of the analytic expression for the half-space Green's function that describes the displacement at any point $\mathbf{x}$ in the bulk due to a unit force acting at another point $\mathbf{x}'$. Then, assuming that the bulk is homogeneously strained, a multipole expansion of the force distribution caused by a step can be made. Multiplying each term in the expansion by the appropriate derivative of the Green's function, the displacement at any point due to the presence of a step can be obtained as well as the force on one step due to another. This is a powerful and appealing approach, but has several serious limitations. The use of the half-space Green's function implies not only that the epilayer is homogeneously strained, but also that the epilayer thickness is much greater than the step height. Furthermore, the distance between steps must also be sufficiently large that the step interactions can be approximated by only a few terms in the multipole expansion. Finally, if the material system is inhomogeneous, then depending on the geometry and elastic parameters, the Green's function approach may be either difficult or impractical to implement.

These restrictions cause problems if the issue to be addressed is the interaction between steps on very thin epilayers on a vicinal substrate, or the interaction between islands on the

first few epilayers on a singular surface. In many cases of practical interest, heteroepitaxial layers are tunnel barriers or quantum wells whose thickness is often no more than a few layers. On a vicinal surface, the presence of steps on the substrate causes the assumption of homogeneity of the epilayer strain to be violated. Even on nominally singular surfaces, the epilayers can easily be thin enough to violate the assumption that the step height is much bigger than the epilayer thickness. The initial nucleation of quantum dots is of intense interest and also occurs in a regime where the Green's function is not valid. The epilayer is thin in the nucleation phase and island distances may be small enough to violate the assumptions of the multipole expansion. Our approach suffers from none of these restrictions and, assuming that linear elasticity holds down to length scales of a few lattice spacings as has been observed[31,32], our only approximations are in the treatment of the atomistic effects relevant very near the step edges and at the surface. Even these effects can be accommodated with some additional effort as described in Sec. V.

IV. RESULTS AND DISCUSSION

As an illustration of our method, we now consider step relaxations and step-step interactions on strained vicinal surfaces.

A. Step relaxations

We begin by examining the behavior of the displacement and strain fields given by our model for steps on a strained vicinal surface. Figure 1 shows the basic geometry that will be considered. The epilayer consists of 40 layers of material with isotropic elastic constants $\lambda = 1$ and $\mu = 1$ on a substrate of thickness 20, which also has elastic constants $\lambda = \mu = 1$. The buried step on the interface between substrate and epilayer is horizontally offset from the surface step to indicate a generic non-symmetric configuration. Although only one step is shown, skew-periodic boundary conditions are applied so that the model describes an infinite step train, not an isolated step.

For clarity we will examine the effects of surface stress as a separate case from epilayer mismatch, with the knowledge that the effects can be combined if desired. For the case of epilayer misfit with no surface stress, there is a lattice mismatch of 1% between substrate and

epilayer with sign such that the epilayer is under compressive strain. For the alternate case of surface stress with no epilayer misfit, only the surface bonds are given a 1% compressive mismatch. In this case, the substrate and epilayer are indistinguishable, so that the system is effectively a layer of thickness 60 with a step on the top and on the bottom.

Figure 2 shows the x and y components of displacement produced by the epilayer misfit model for this particular step configuration, and Figure 3 shows the displacements for the surface-stress only case. Better qualitative appreciation of the results of the relaxation can be gained from graphing the components of the strain tensor. Figure 4, for the compressed epilayer, clearly shows the distinct strain fields produced by the surface step and the buried interface step. Of note is the different "polarity" of the x- and y-strains of the surface step vs. the interface step, and the angular $(-+-+)$ structure around each of the steps. Figure 5 shows the strains produced by surface stress only. In this case, the buried step experiences no strain, and the visible strain field is due to the surface step alone. The angular structure around the step in (a) and (c) is noticeably different, suggesting more dominant higher multipole moments.

B. Isolated and Periodic Step Train Comparisons

The Green's function method[29,30] predicts the displacement and strain fields caused by an isolated step on a uniformly strained substrate. The present method naturally includes the effects of buried steps between the epilayer and substrate, as well as periodically placed steps in a step train. In order to separate the effect of an isolated step from that of the periodic images, we perform a lattice sum of periodic multipole forces, which is then used for evaluation of the multipole coefficients at an step in Section IV B 1. The effect of epilayer thickness is demonstrated by computation of elastic energy for two systems with large and small epilayer thickness in Section IV C. A more complete assessment of the effect of epilayer and substrate thickness will be the subject of a future work.

1. Lattice-Summed Multipole Functions

The effect of a single isolated step in an (horizontally) infinite domain is addressed by superposition in periodic boundary conditions. The computational domain, when skew-

periodic boundaries are applied, is effectively infinite, and is populated by an infinite number of equally spaced steps. The distortion fields produced by each of these steps linearly superposes, however, and may be summed. For example, a one dimensional "dipole potential" term[52] of strength m_1 for an isolated step at x_0,

$$V_1^1 = \frac{m_1}{x - x_0} \tag{15}$$

sums as

$$V_1^\infty = \sum_{n=-\infty}^{\infty} \frac{m_1}{x - x_0 + nL} = m_1 \frac{\pi}{L} \cot\left(\frac{\pi}{L}\ (x - x_0)\right), \tag{16}$$

where L is the periodicity of the system. The summed dipole force is found as the negative derivative of the potential:

$$f_1^\infty = -\frac{d}{dx} V_1^\infty = m_1 \left(\frac{\pi}{L}\right)^2 \csc^2\left(\frac{\pi}{L}(x - x_0)\right). \tag{17}$$

All higher order multipole terms may be summed analogously. The single step monopole potential term,

$$V_0^1 = m_0 \log(x - x0) \tag{18}$$

can not be directly summed and instead the corresponding *force*

$$f_0^1 = -\frac{d}{dx} V_0^1 = \frac{m_0}{x - x0} \tag{19}$$

is summed, and then integrated to give the lattice-summed monopole potential

$$V_0^\infty = m_0 \log\left(\sin\left(\frac{\pi}{L}(x - x0)\right)\right). \tag{20}$$

These periodic functions are best examined on a single period extending over the *terrace* between two steps (Figure 6), and not on a domain containing a pole, which would require fitting with an infinite discontinuity between left- and right-hand sides.

The coefficients m_0, m_1, m_2, etc. of these lattice-summed terms are identical to the coefficients of the isolated step continuum multipole expansion. This allows the coefficients from a fit to our model on a terrace to be compared directly to the coefficients derived from the continuum theory for a single step.

2. Strained Epilayer

Figure 6 shows the x and y displacements along a terrace for the case of a uniformly compressed epilayer. From the fit we can extract the multipole coefficients of the isolated step. The spectrum of the first 12 multipole coefficients is shown in Figure 7.

Figure 8 shows the monopole coefficient $M0_x$ for the x component of the displacement along the surface. Results from a fit to the simulation, as described above, are compared to the theoretical prediction, which can be taken either from continuum theory or from a discrete model[27].

C. Step-step interaction energy

For a general linear elastic material with a stepped surface, there are forces between steps even in the absence of misfit strain. In the Green's function approach discussed above, these forces separate (conceptually) into two types: a repulsive "dipole" interaction[39], which is due to the intrinsic surface stress of the steps, and a logarithmic repulsion between inequivalent steps in the form of a force "monopole"[40,41], which is due to the elastic distortion of the surface.

In a film under an externally imposed strain, such as that derived from coherent epitaxy to a lattice-mismatched substrate material, there is an additional, *attractive* interaction between steps due to a force "monopole"[41] which is logarithmic. The unstrained monopole force of the previous paragraph is fundamentally different from this strained monopole, in that the presence or absence of the former depends on relative step orientations, while the latter is present for all steps. In the calculations described below, all steps face the same direction, obviating any repulsive monopole.

The force f_m on a single step at position x_m is approximated, to dipole order, by[26,29,39]

$$f_m = \sum_{\substack{n \\ n \neq m}} \left(\frac{m_1}{(x_n - x_m)} - \frac{m_2}{(x_n - x_m)^3} \right), \tag{21}$$

where m_1 is determined by the elastic constants of the materials and the lattice mismatch, and m_2 is determined by the elastic constants of the epilayer material and the intrinsic surface stresses.

In light of the above discussion, we now compare the elastic energy due to step-step interaction obtained in our model to the predicted interaction. To calculate the total elastic

energy as a function of step distance, we use the geometry shown in Fig. 9, with skew periodic boundary conditions as appropriate for modeling an infinite step train. The two steps are moved in equal and opposite directions to conserve the mass of the system, thereby preventing the uncontrolled introduction of "background" bulk elastic energy in the process. With the steps at each lattice position between configurations A and B, we record the total elastic energy.

We expect that the relevant quantities determining the qualitative behavior of the system are μ_i/λ_i and μ_s/μ_e, where the subscripts s and e are for substrate and epilayer properties, and $i \in \{s, e\}$. Every property that depends on lattice mismatch ϵ depends linearly, so that scales out as well. For simplicity we calculate with $\lambda = \mu = 1$, and $\epsilon = 1\%$. For Si, $\mu/\lambda \approx 1.1$; for Ge, $\mu/\lambda \approx 1.2$, and $\mu_{\mathrm{Si}}/\mu_{\mathrm{Ge}} \approx 1.2$, so the qualitative results should hold for that physical system and others with similar scaled elastic properties. In this computation, the grid spacing was chosen such that each atomic lattice spacing is one numerical grid point across. The system has a lateral size of 40 lattice spacings, which would be equivalent to a physical size of approximately 22 nm for a Si/Ge system.

The first case we consider has an epilayer thickness of 30 ML, large enough that we expect this case to behave as a uniformly strained epilayer. The results for the total energy as a function of step separation are shown by the square data points in Fig. 10. The agreement between the data from our model and the solid line is excellent, indicating that our model reproduces the expected logarithmic interaction between steps on a homogeneously strained epilayer at distances larger than one atom.

The circle data points in Figure 10 show the total elastic energy for an epilayer thickness of only 5 ML. Note that the behavior is qualitatively different than the thick epilayer case. There is a "dip" in the energy as the surface steps pass over the terrace midway between configurations A and B. This local minimum in energy becomes more pronounced for epilayers thinner than 5 monolayers. Fig. 11 shows the hydrostatic strains for two of the configurations whose energies are plotted in the preceding figure. Note that there is significant elastic interaction between the epilayer steps and subsurface features at the epilayer-substrate interface. This interaction is what leads to the local minimum in energy when the epilayer steps are moved with respect to the buried steps, and is an effect not present in models assuming a homogeneously strained epilayer. In fact, this effect would be very difficult to capture with any Green's function-based approach.

We expect this to have considerable implications for the dynamics of step bunching. Although only metastable, step configurations that experience significant coupling to the substrate may be expected to slow or even completely suppress the step bunching phenomenon normally expected on vicinal surfaces even under annealing conditions. (We might want to mention here that step bunching is almost never seen in the thin epilayers grown for quantum wells or barrier layers in device heterostructures.) A full investigation of step dynamics using this elastic model coupled to an equilibrium model for step dynamics[29] is in progress will be reported on elsewhere.

V. SUMMARY AND FUTURE APPLICATIONS

We have presented a new method to study the influence of elastic interactions in strained one-dimensional systems using an approach based on lattice statics using linear elasticity theory. An application is the problem of step relaxations and step-step interactions on vicinal surfaces. We have examined in detail the behavior of our model for this particular problem and found the step relaxations to be consistent with the predictions of continuum elastic theory in the limit where the continuum theory would be expected to hold (the thick epilayer limit). We have also demonstrated, however, that the discrete nature of the model allows us to capture many effects that are essentially atomistic in nature. When considering step-step interactions, we found that there is a significant influence of perturbations of the elastic field on the surface due to buried substrate morphologies. These may well lead to long relaxation times for very thin epilayers, where the actual critical thickness depends on the misfit ϵ as well as on the elastic constants of the two involved materials. Upon increase of the epilayer thickness, we observe a decay of the substrate influence until at epilayer heights of roughly 30-50 monolayers the effects of the initial substrate configuration vanish.

We expect this general methodology to have wide applicability to problems involving strain in epitaxial growth. Here, the method was formulated for a simple cubic lattice in 2D, but it is easily extendible to non-cubic lattices and 3D. In addition, the atomistic nature of our formulation makes it applicable to including surface and step edge effects, provided that a suitable description of the local energy at these sites is available. At the atomistic level, our model is an example of a valence force field model. Valence force field models, such as the Keating model, have been validated for bulk elastic properties of many real

materials[28,46,47]. Valence force field models accurately describing the energy of atomic configurations at surfaces and step edges are not generally available, but there are no fundamental obstacles to developing and validating such models.

One of the main motivations for this work is our intention of incorporating elastic effects into the level-set method[48] for describing the morphological evolution of epitaxial films[49]. This technique is based on the representation of the moving growth front (the step edges) in terms of an auxiliary function (the level set function) which permits a straightforward solution of the associated Stefan problem and handles in a natural way the topological changes associated with the nucleation of islands and their coalescence. By treating the x–y variables as continuous, but the z direction as discrete, this method is ideally suited both to coupling continuous fields to island motion and to describing abrupt atomistic effects associated with the initial stages of heteroepitaxial growth, such as the 2D–3D transition during Stranski–Krastanov growth[50]. The coupling of the adatom diffusion field to island-boundary motion has already been accomplished[51], so we now turn to the effect of elasticity on the motion of island boundaries.

The new method opens up a vast field of possible applications, such as spatial ordering effects in heterogeneous multilayer systems and the representation of compositional gradients through introducing a layer dependent ϵ. We expect to apply this methodology to problems in 3D island growth and island ordering, quantum dots, Stranski-Krastanov growth, periodically faceted surfaces, and many other problems involving stress effects in epitaxial growth.

Acknowledgments

We gratefully acknowledge discussions with Frank Grosse, David Srolovitz and Jerry Tersoff. This work was supported by the NSF and DARPA through cooperative agreement No. DMS-9615854 as part of the Virtual Integrated Prototyping Initiative, the NSF through Focused Research Grant (FRG) No. DMS-0074152, and by the (UK) EPSRC. A.C.S. was supported by a DAAD Fellowship within "Hochschulsonderprogramm III von Bund und Ländern" (Germany).

APPENDIX A: ELASTIC ENERGY

For a two-dimensional cubic lattice with lattice constant h and lattice coordinates $\boldsymbol{i} = (i_1, i_2)$, denote the reference position as $\boldsymbol{x} = (x_1, x_2)$, the elastically deformed position as $\boldsymbol{X} = (X_1, X_2)$ and the displacement as $\boldsymbol{u} = (u_1, u_2) = \boldsymbol{X} - \boldsymbol{x}$. Define the translation operators $T_k^{\pm}$ and finite-difference operators $D_k^{\pm}, D_k^0$ as follows:

$$\begin{aligned} T_k^{\pm} f(\boldsymbol{i}\,) &= f(\boldsymbol{i} \pm \mathbf{e}_k) && \text{(A1)} \\ D_k^{+} f(\boldsymbol{i}\,) &= h^{-1}(T_k^{+} - 1) f(\boldsymbol{i}\,) \\ D_k^{-} f(\boldsymbol{i}\,) &= h^{-1}(1 - T_k^{-}) f(\boldsymbol{i}\,) && \text{(A2)} \\ D_k^{0} f(\boldsymbol{i}\,) &= (2h)^{-1}(T_k^{+} - T_k^{-}) f(\boldsymbol{i}\,). \end{aligned}$$

in which $\mathbf{e}_k$ is the unit vector in the k-th direction for $k = 1, 2$. Define the bond displacement $\mathbf{d}^{k\pm}$ at the point $\boldsymbol{i}$ as

$$\mathbf{d}^{k\pm}(\boldsymbol{i}\,) = (d_1^{k\pm}, d_2^{k\pm}) = D_k^{\pm} \boldsymbol{u}\,(\boldsymbol{i}\,) - \epsilon \mathbf{e}_k. \tag{A3}$$

As discussed in Section II, the lattice mismatch parameter ϵ in the epilayer is the relative difference between the equilibrium lattice constant and the lattice constant imposed on the epilayer by the substrate.

The discrete strain components at a point $\boldsymbol{i}$ are defined as

$$\begin{aligned} S_{kk}^{\pm} &= d_k^{k\pm} \\ S_{k\ell}^{pq} &= (d_k^{\ell q} + d_\ell^{kp})/2 && \text{(A4)} \end{aligned}$$

in which the values of k and ℓ are 1 or 2 and the values of p and q are $+$ or $-$. The strain component $S_{kk}^{\pm}$ corresponds to a bond in the $\pm\mathbf{e}_k$ direction from the point $\boldsymbol{i}$; the component $S_{k\ell}^{pq}$ corresponds to two interacting orthogonal bonds in the $p\mathbf{e}_k$ and $q\mathbf{e}_\ell$ directions from the point $\boldsymbol{i}$.

1. Micro-Mechanical Model

The elastic energy used here has a micro-mechanical interpretation as consisting of nearest neighbor springs, diagonal springs and bond bending terms. For nearest neighbor linear

springs and linearized bond bending springs, in which the spring constants are a and b respectively, the energy at a point is

$$E_{nnbb} \;=\; \tfrac{1}{2}a \sum_{p=\pm,k=1,2} (S^p_{kk})^2 + \tfrac{1}{2}b \sum_{p=\pm,q=\pm} (S^{pq}_{12})^2. \tag{A5}$$

In order to retain maximal locality, we use "virtual" diagonal spring with spring constant c, defined for example between a point $(0,0)$ and the average of its nearest neighbors $(1,0)$ and $(0,1)$, for which the energy is

$$E^{++} = \tfrac{1}{2}c((\mathbf{e}_1+\mathbf{e}_2)\cdot((\boldsymbol{u}\,(1,0)+\boldsymbol{u}\,(0,1))/2-\boldsymbol{u}\,(0,0))^2 = c(S^+_{11}+S^+_{22}+2S^{++}_{12})^2/8. \tag{A6}$$

More generally for $p=\pm, q=\pm$ define

$$E^{pq} = c(S^p_{11}+S^q_{22}+2pqS^{pq}_{12})^2/8 \tag{A7}$$

The energy density E is a combination of these four virtual diagonal springs; i.e.

$$E = \sum_{p=\pm,q=\pm} E^{pq}. \tag{A8}$$

Add and rearrange (A5) and (A8), to obtain the resulting energy

$$E \;=\; \alpha \sum_{p=\pm,k=1,2} (S^p_{kk})^2 + \sum_{p=\pm,q=\pm} \{\beta(S^{pq}_{12})^2 + \gamma S^p_{11}S^q_{22}\} \tag{A9}$$

in which

$$\begin{aligned} \alpha \;&=\; (a+c)/2 = C_{11}/2 \\ \beta \;&=\; (b+c)/2 = C_{44}/2 \\ \gamma \;&=\; c/8 = C_{12}/2. \end{aligned} \tag{A10}$$

and C_{ij} are the Voigt constants. The energy density (A9) is the discrete analogue of the continuum energy for elasticity with cubic symmetry. For isotropic elasticity, as in Section II, the coefficients should be chosen as

$$\begin{aligned} \alpha \;&=\; (\lambda+2\mu)/2 \\ \beta \;&=\; \mu/2 \\ \gamma \;&=\; \lambda/2 \end{aligned} \tag{A11}$$

i.e. $a=\mu-2\lambda, \quad b=\mu-4\lambda, \quad c=4\lambda.$

The discrete energy density (A9) has been chosen to be maximally localized; so that the energy density E at a point $\boldsymbol{i}$ is a quadratic function of displacement $\boldsymbol{u}$ at the five point stencil consisting of the point $\boldsymbol{i}$ and its nearest neighbors, and the corresponding force balance equations involve only the nine point stencil consisting of the point $\boldsymbol{i}$ and its nearest and next-nearest neighbors.

2. Interfaces

For problems in which the underlying lattice has cubic symmetry but the material geometry includes interfaces, we generalize the energy in (A9) by only keeping bond interactions that are consistent with cubic symmetry but not imposing a symmetry constraint on the strength of the interactions. The resulting energy has the form

$$E = \sum_{p=\pm,k=1,2} \alpha_k^p (S_{kk}^p)^2 + \sum_{p=\pm,q=\pm} \beta^{pq} (S_{12}^{pq})^2 + \gamma^{pq} S_{11}^p S_{22}^q \tag{A12}$$

Each coefficient α_k^p, as well as the lattice mismatch parameter ϵ, corresponds to a bond between two atoms; each of the coefficients β^{pq} and γ^{pq} corresponds to the interaction of two bonds in orthogonal directions from a central point, which defines a square "cell". We assume that the values of $\alpha_k^{\pm}$ and ϵ (β^{pq} and γ^{pq}) depend only on the material type of the two (four) atoms at the endpoints of the corresponding bond (cell).

Consider a system consisting of two materials with elastic parameters $\alpha^m, \beta^m, \gamma^m, \epsilon^m$ for $m = 1, 2$. Denote a cell or bond to be "pure" if all of its vertices are of a single material type and "mixed" otherwise. For maximal simplicity, we make the following assumptions, which could easily be generalized:

1. For pure bonds (pure cells) in material m, $\alpha_k^p = \alpha^m$ and $\epsilon = \epsilon^m$, ($\beta^{pq} = \beta^m$ and $\gamma^{pq} = \gamma^m$).

2. For mixed bonds (mixed cells) in a two-material system, $\alpha_k^p = \frac{1}{2}(\alpha^1 + \alpha^2)$ and $\epsilon = \frac{1}{2}(\epsilon^1 + \epsilon^2)$ ($\beta^{pq} = \frac{1}{2}(\beta^1 + \beta^2)$ and $\gamma^{pq} = \frac{1}{2}(\gamma^1 + \gamma^2)$).

3. For a bond (cell) in which one of the vertices is in the vacuum, $\alpha_k^p = 0$ ($\beta^{pq} = \gamma^{pq} = 0$).

3. Force Balance Equations

Assumptions (1)-(3) provide an algorithm by which the elastic coefficients and elastic energy can be determined for any material configuration involving two materials (i.e. a substrate and an epilayer) and a vacuum. Once the energy E is determined, the force balance equations at each point $\boldsymbol{i}$ are the minimization conditions

$$\partial E/\partial \boldsymbol{u}\ (\boldsymbol{i}\ ) = 0. \tag{A13}$$

For the quadratic energy described above, the derivative in (A13) is a linear function of $\boldsymbol{u}\ (\boldsymbol{i}\ ')$ over values of $\boldsymbol{i}\ '$ that are equal to, nearest neighbors of, or next-nearest neighbors of $\boldsymbol{i}$. The coefficients can exactly determined as a finite difference of E with respect to $\boldsymbol{u}\ (\boldsymbol{i}\ )$ and $\boldsymbol{u}\ (\boldsymbol{i}\ ')$. Then a linear equation solver is used to find $\boldsymbol{u}$ by solving (A13). This procedure does not require analytic determination of the force balance equation, which is an advantage because the analysis has many different cases[27].

---

[1] E. Bauer, Z. Krist. **110**, 372 (1958).

[2] D. Leonard, M. Krishnamurthy, C. M. Reaves, S. P. DenBaars, and P. M. Petroff, Appl. Phys. Lett. **63**, 3203 (1993); J. M. Moison, F. Houzay, F. Barthe, and L. Leprince, Appl. Phys. Lett. **64**, 196 (1994); A. Madhukar, Q. Xie, P. Chen, and A. Konkar, Appl. Phys. Lett. **64**, 2727 (1994); R. Leon, T. J. Senden, Y. Kim, C. Jagadish, and A. Clark, Phys. Rev. Lett. **78**, 4942 (1997); Y. Ebiko, S. Muto, D. Suzuki, S. Itoh, K. Shiramine, T. Haga, Y. Nakata, and N. Yokoyama, Phys. Rev. Lett. **80**, 2650 (1998).

[3] W. K. Burton, N. Cabrera and F. C. Frank, Philos. Trans. Roy. Soc. London, Sect. A **243**, 299 (1951).

[4] J. A. Venables, G. D. T. Spiller and M. Hanbucken, Rep. Prog. Phys. **47**, 399 (1984).

[5] J. D. Weeks and G. H. Gilmer, Adv. Chem. Phys. **40**, 157 (1979); S. Clarke and D. D. Vvedensky, Phys. Rev. Lett. **58**, 2235 (1987); A. Madhukar and S. V. Ghaisas, CRC Crit. Rev. Sol. State and Mater. Sci. **14**, 1 (1988); H. Metiu, Y.-T. Lu, and Z. Y. Zhang, Science **255**, 1088 (1992); H. C. Kang and W. H. Weinberg, J. Chem. Phys. **90**, 2824 (1989).

[6] C. Ratsch and A. Zangwill, Surf. Sci. **293**, 123 (1993).

[7] C. Ratsch, P.Šmilauer, D. D. Vvedensky, and A. Zangwill, J. Phys. I (France) **6**, 575 (1996).

[8] H. M. Koduvely and A. Zangwill , Phys. Rev. B **60** R2204 (1999).

[9] F. K. LeGoues, MRS Bulletin, **21**(4), 38 (1996); B. A. Joyce, J. L. Sudijono, J. G. Belk, H. Yamaguchi, X. M. Zhang, H. T. Dobbs, A. Zangwill, D. D. Vvedensky and T. S. Jones, Jpn. J. Appl. Phys. **36**, 4111 (1997).

[10] V. A. Shchukin and D. Bimberg, Rev. Mod. Phys. **71**, 1125 (1999).

[11] M. Schneider, I. K. Schuller, and A. Rahman, Phys. Rev. B **36**, 1340 (1987); M. H. Grabow and G. H. Gilmer, Surf. Sci. **194**, 333 (1988); B. W. Dodson, CRC Crit. Rev. Sol. State and Mater. Sci. **16**, 115 (1990).

[12] A. Kobayashi, S. M. Paik, and S. Das Sarma, J. Vac. Sci. Technol. B **6**, 1145 (1988); D. A. Faux, G. Gaynor, C. L. Carson, C. K. Hill, J. Bernholc, Phys. Rev. B **42**, 2914 (1990); B. G. Orr, D. Kessler, C. W. Snyder, and L. Sander, Europhys. Lett. **19**, 33 (1992). A. Madhukar, J. Cryst. Growth **163**, 149 (1996).

[13] D. A. Faux, G. Gaynor, C. L. Carson, C. K. Hall, and J. Bernholc, Phys. Rev. B **42**, 2914 (1990); J. Kew, M. R. Wilby, and D. D. Vvedensky, J. Crystal Growth **127**, 508 (1993); F. Much, M. Ahr, M. Biehl, W. Kinzel, `cond-mat/0106435`.

[14] B. J. Spencer, P. W. Voorhees, and S. H. Davis, Phys. Rev. Lett. **67**, 3696 (1991); B. J. Spencer, P. W. Voorhees, and S. H. Davis, J. Appl. Phys. **73**, 4955 (1993); B. J. Spencer, S. H. Davis, and P. W. Voorhees, Phys. Rev. B **47**, 9760 (1993).

[15] P. Politi, G. Grenet, A. Marty, A. Ponchet, J. Villain, Rep. Prog. Phys. **324**, 271 (2000).

[16] M. Born and K. Huang *Dynamical theories of crystal lattices*, Oxford U. Press, 1954.

[17] M. Ortiz and R. Phillips "Nanomechanics of defects in solids" Adv. Appl. Mech. 36 (1999) 1-79

[18] V.K. Tewary "Green-function method for lattice statics" Adv. Phys. 22(1973) 757-810.

[19] V. S. Stepanyuk, D. I. Bazhanov, W. Hergert, and J. Kirschner, Phys. Rev. B **63**, 153406 (2001).

[20] C. Priester and M. Lannoo, Phys. Rev. Lett. **75**, 93 (1995).

[21] L. G. Wang, P. Kratzer, N. Moll, and M. Scheffler, Phys. Rev. B **62**, 1897 (2000).

[22] J. M. Rickman and D. J. Srolovitz, Surf. Sci. **284** 211 (1993).

[23] K. H. Lau and W. Kohn, Surf. Sci. **65**, 607 (1977).

[24] P. Peyla, A. Vallat, C. Misbah and H. Muller-Krumbhaar, Phys. Rev. Let. **82** 787 (1999).

[25] Y. Saito, H. Uemura, and M. Uwaha, Phys. Rev. B **63**, 045422 (2001).

[26] L. D. Landau and E. M. Lifschitz, *Theory of Elasticity* (Pergamon, Oxford, 1970).

[27] R. E. Caflisch and C. Connell (unpublished).

[28] P. N Keating, Phys. Rev. **145**, 637 (1966).

[29] J. Tersoff, Y. H. Phang, Z. Zhang, and M. G. Lagally, Phys. Rev. Lett. **75**, 2730 (1995).

[30] R.V. Kukta and K. Bhattacharya, Thin Solid Films, **357**, 35 (1999),(MRS Symposium: Growth Instabilities and Decompostion During Heteroepitaxy, Boston, TX, USA, Dec. 1998.)

[31] D. J. Srolovitz, private communication.

[32] I. Daruka, A.-L. Barabási , S. J. Zhou, T. C. Germann, P. S. Lomdahl, and A. R. Bishop, Phys. Rev. B **60**, R2150 (1999).

[33] The thermodynamic principles behind the adatom concentration are discussed at length by A. Pimpinelli and J. Villain, *Physics of Crystal Growth* (Cambridge University Press, Cambridge, 1998).

[34] R.E. Caflisch (unpublished).

[35] D. Kandel and J. D. Weeks, Phys. Rev. Lett. **69**, 3758 (1992); D. Kandel and J. D. Weeks, Phys. Rev. B **49** 5554 (1994).

[36] J. Frohn, M. Giesen, M. Poensgen, J. F. Wolf, and H. Ibach, Phys. Rev. Lett. **67**, 3543 (1991).

[37] A. C. Redfield and A. Zangwill, Phys. Rev. B **46**, 4289 (1992).

[38] C. Duport, P. Noziéres, and J. Villain, Phys. Rev. Lett. **74**, 134 (1995).

[39] V. I. Marchenko and A. Ya. Parshin, Sov. Phys. JETP **52**, 129 (1980).

[40] V. I. Marchenko, JETP Lett. **33.** 381 (1981).

[41] O. L. Alerhand, D. Vanderbilt, R. D. Meade, and J. D. Joannopoulos, Phys. Rev. Lett. **61**, 1973 (1988).

[42] `http://math.nist.gov/sparselib`

[43] Our model does not exhibit a repulsive interaction between steps because we have not included the intrinsic surface stress that is responsible for this repulsion. The incorporation of the linear elastic effects that are necessary to obtain the short-range repulsion is straightforward and will be described in a future publication.

[44] J. Stewart and N. D. Goldenfeld, Phys. Rev. A **46**, 6505 (1992).

[45] F. Liu, J. Tersoff and M. G. Lagally, Phys. Rev. Lett. **80**, 1268 (1998).

[46] R. M. Martin, Phys. Rev. B **1**, 4005 (1970).

[47] F. Grosse and J. Neugebauer, Phys. Rev. B **63**, 085207 (2001).

[48] S. Osher and J. A. Sethian, J. Comput. Phys. **79**, 12 (1988); S. Chen, B. Merriman, S. Osher, and P. Smereka, J. Comput. Phys. **135** 8, (1997).

[49] M. F. Gyure, C. Ratsch, B. Merriman, R. E. Caflisch, S. Osher, J. J. Zinck, and D. D. Vvedensky, Phys. Rev. E **58**, R6927 (1998).

[50] W. Seifert, N. Carlsson, M. Miller, M.–E. Pistol, L. Samuelson and L. R. Wallenberg, Prog. Crystal Growth and Charact. **33**, 423 (1996).

[51] C. Ratsch, M. F. Gyure, S. Chen, M. Kang, and D. D. Vvedensky, Phys. Rev. B **61**, R10 598 (2000).

[52] We use the notation m_0, m_1, etc. to represent coefficients of the monopole, dipole, etc., respectively. The numbering is meant to represent the power of x in the denominator of the single-step term.

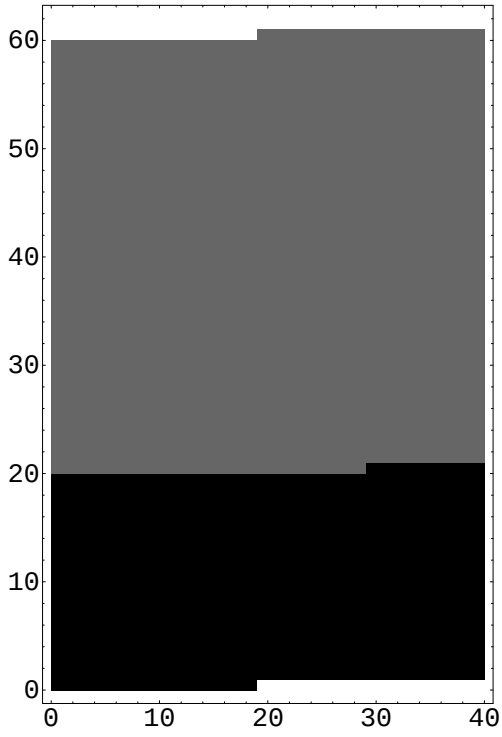

FIG. 1: A vicinal surface with a single step consisting of an epilayer of A-type atoms on a substrate of B-type atoms.

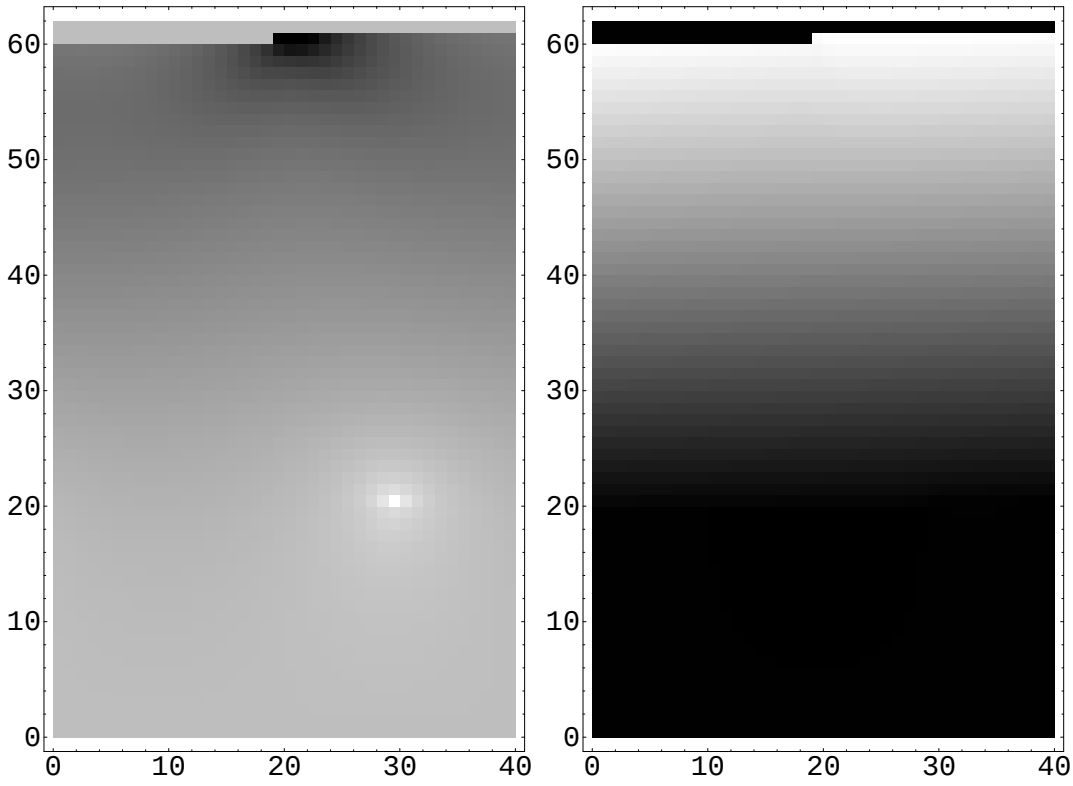

FIG. 2: Displacement fields due to a step on a compressively strained epilayer. White represents large positive displacements and black represents large negative displacements. The x-displacements are shown in (a) and the y-displacements are shown in (b).

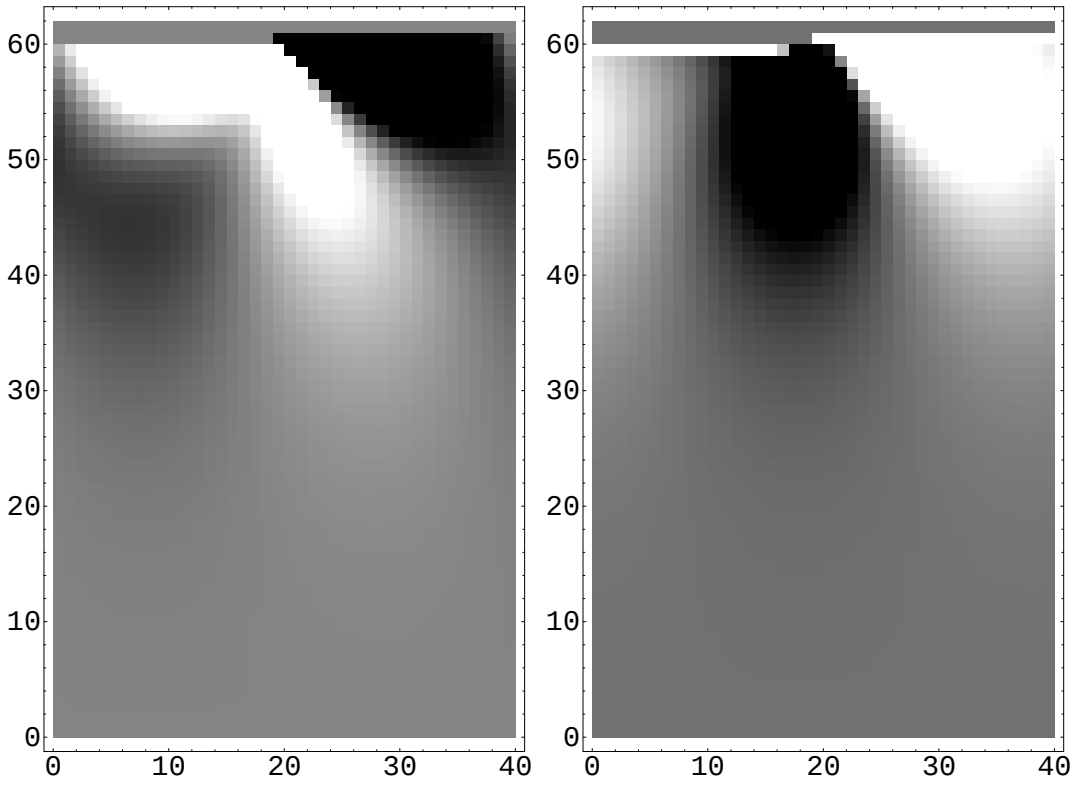

FIG. 3: Displacement fields due to a step with intrinsic surface stress in the material. The black–white gradient is not to the same scale as Figure 2. The x-displacements are shown in (a) and the y-displacements are shown in (b).

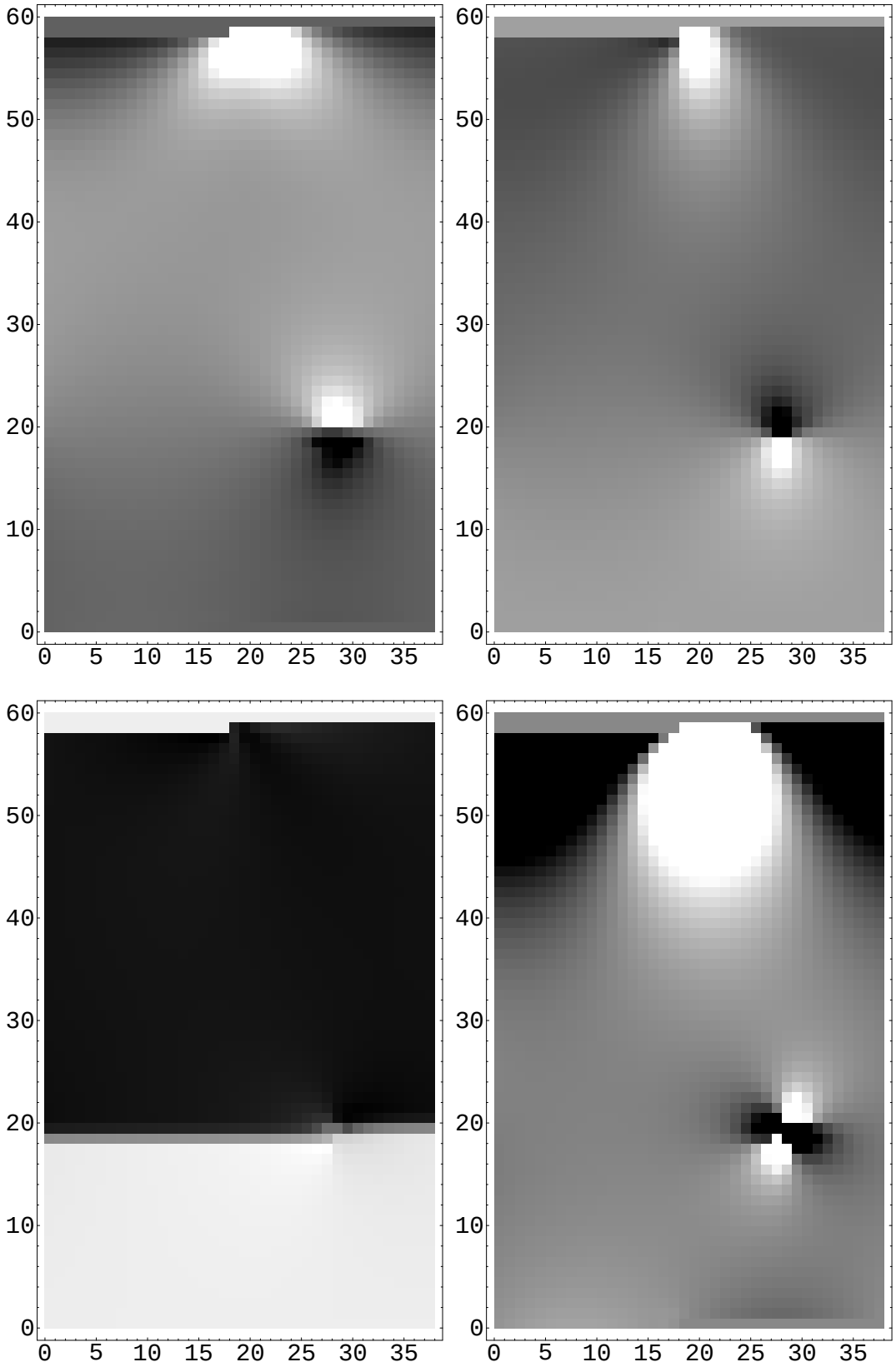

FIG. 4: Components of the strain field due to a step with intrinsic surface stress in the material, with geometry. The components shown are as follows: (a) xx-component, (b) yy-component, (c) xy-component and (d) hydrostatic strain (trace of strain tensor). The white represents large positive strains and the black, large negative strains.

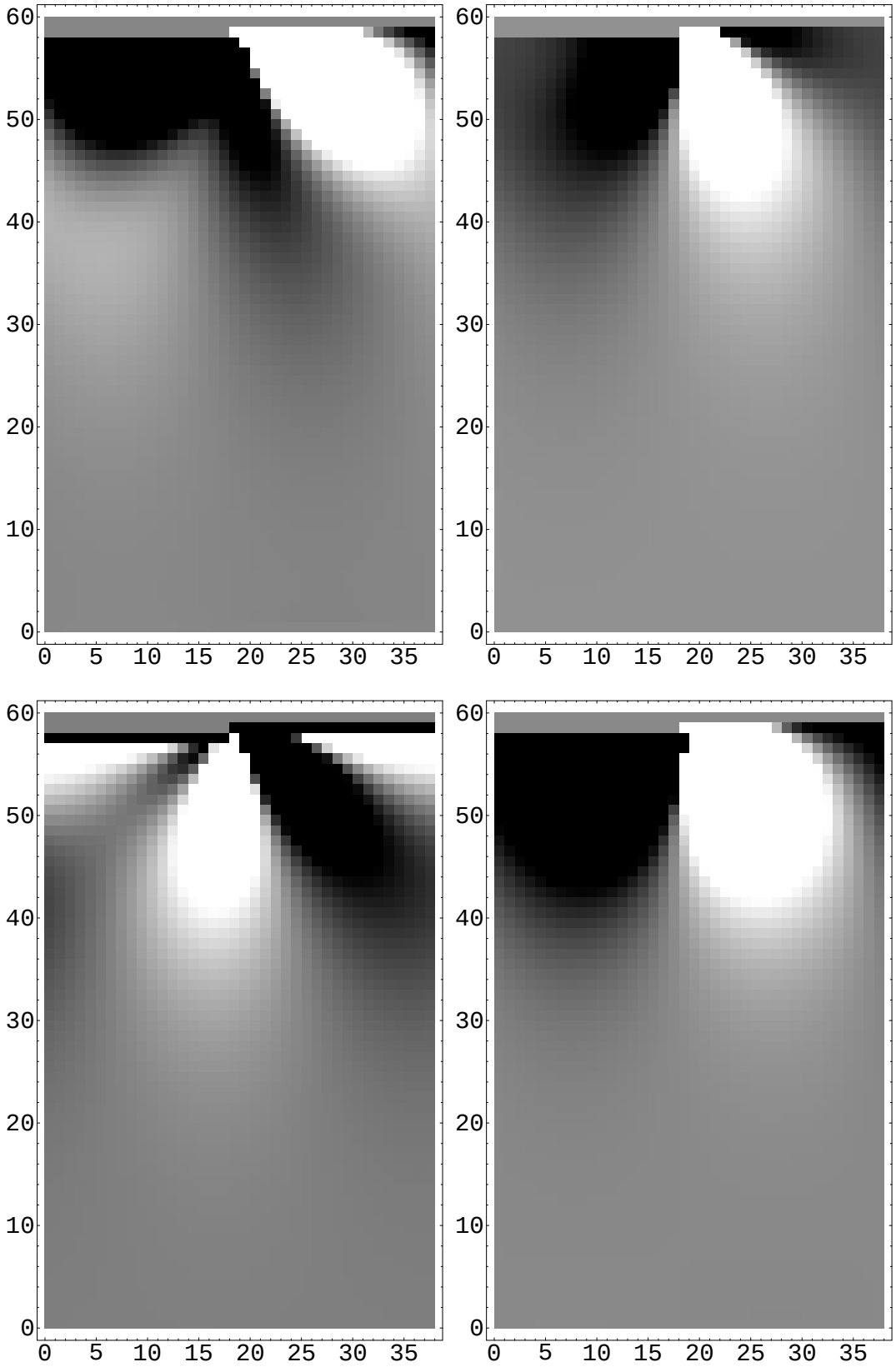

FIG. 5: Components of the strain field due to a step on a compressively strained epilayer. The components shown are as follows: (a) xx-component, (b) yy-component, (c) xy-component and (d) hydrostatic strain (trace of strain tensor). The white represents large positive strains and the black, large negative strains.

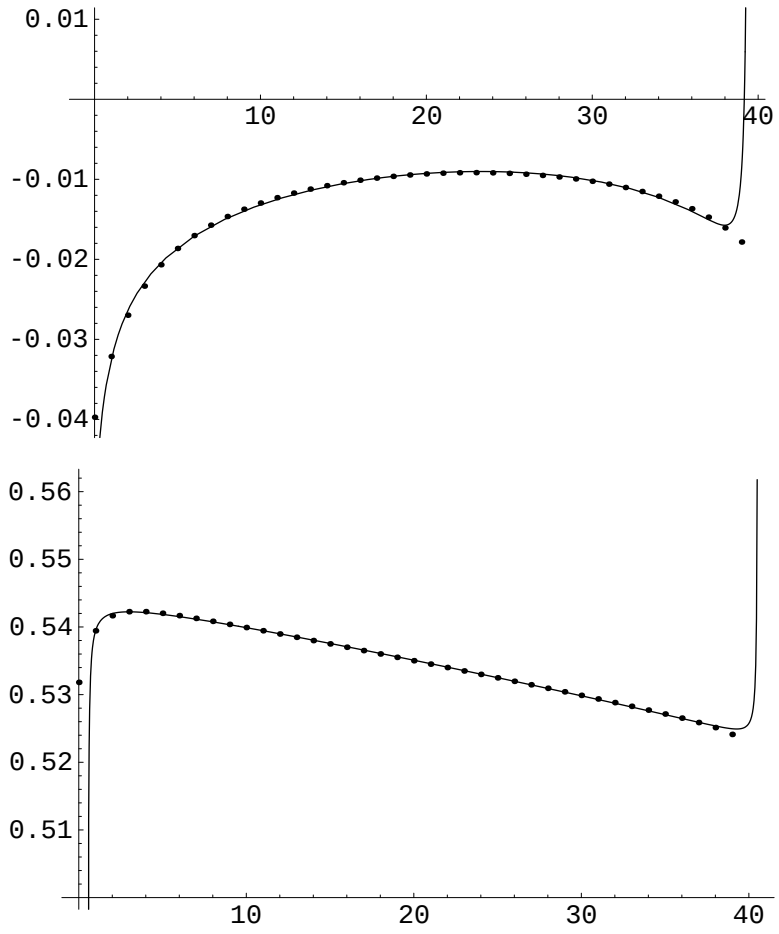

FIG. 6: Displacements at the surface layer (from Figure 2), for a strained epilayer with no surface stress. x displacements (a) and y displacements (b) are shown as a function of position from one step to the next periodic image step. The dots are the displacements produced by the model and the solid lines are fits to the function described in the text, up to dipole order. (The first and last points are left out of the fit.)

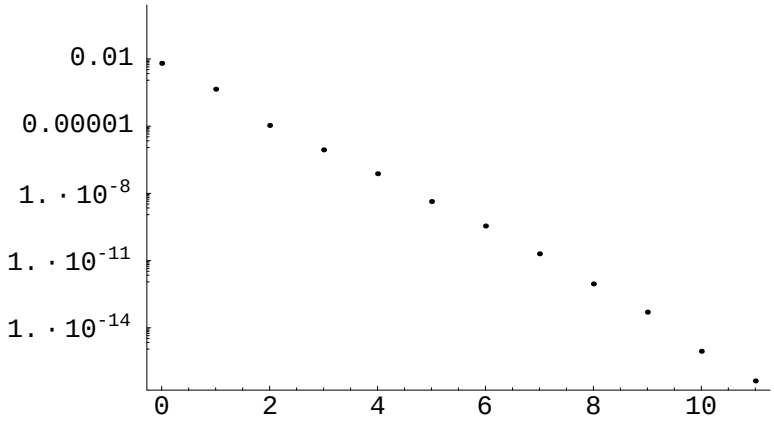

FIG. 7: Magnitude of x-displacement multipole coefficients for first 12 multipoles, $m_0 ... m_{11}$, for a strained epilayer with no surface stress. The logarithmic monopole is dominant, and the falloff with increasing multipole order is rapid and uniform. y-displacement multipoles are similar.

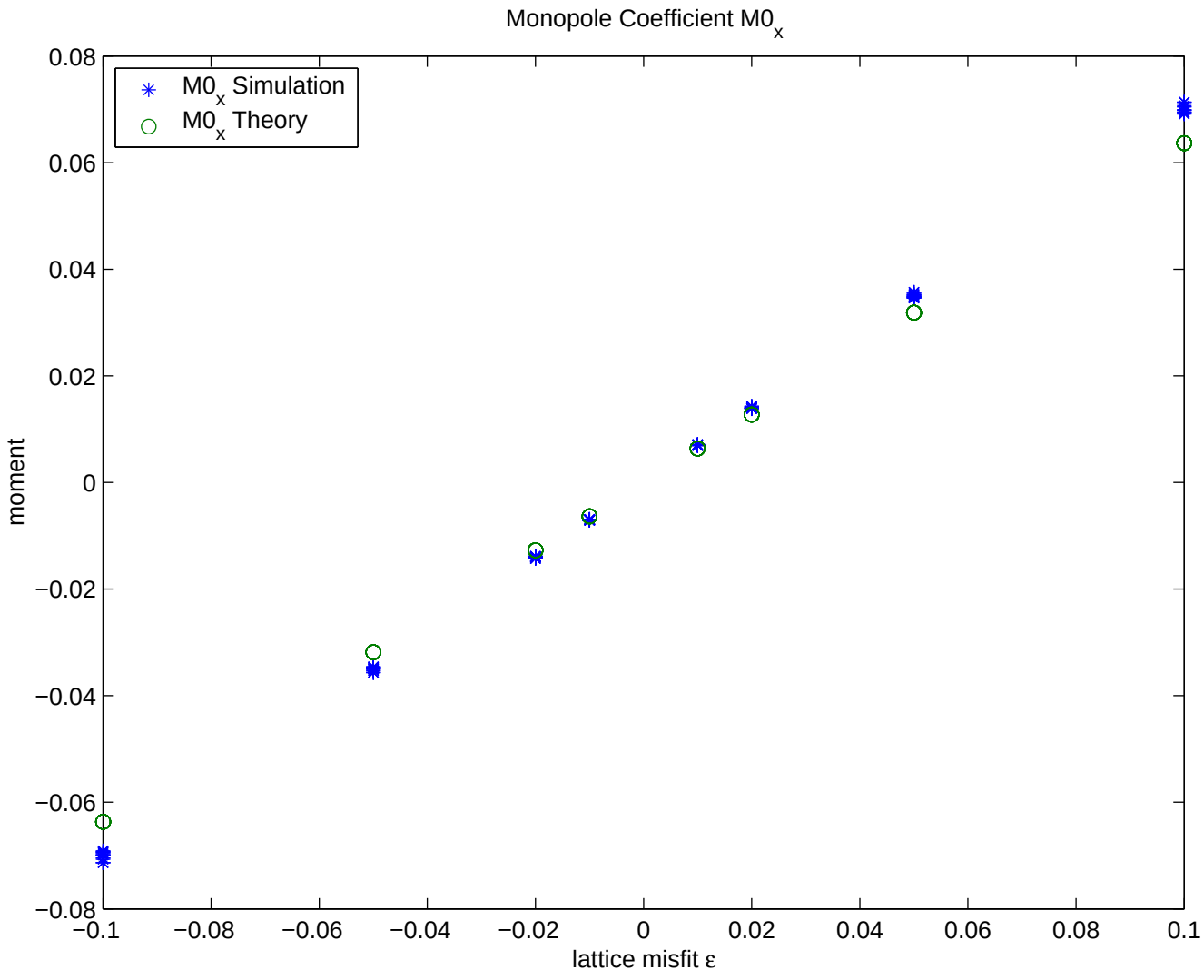

FIG. 8: Monopole coefficient $M0_x$ for the x component of the displacement along the surface. Plotted as a function of lattice misfit ϵ for 128 values of elastic coefficients λ , μ and ϵ. Values from the simulation (*) and from theory (o) are plotted.

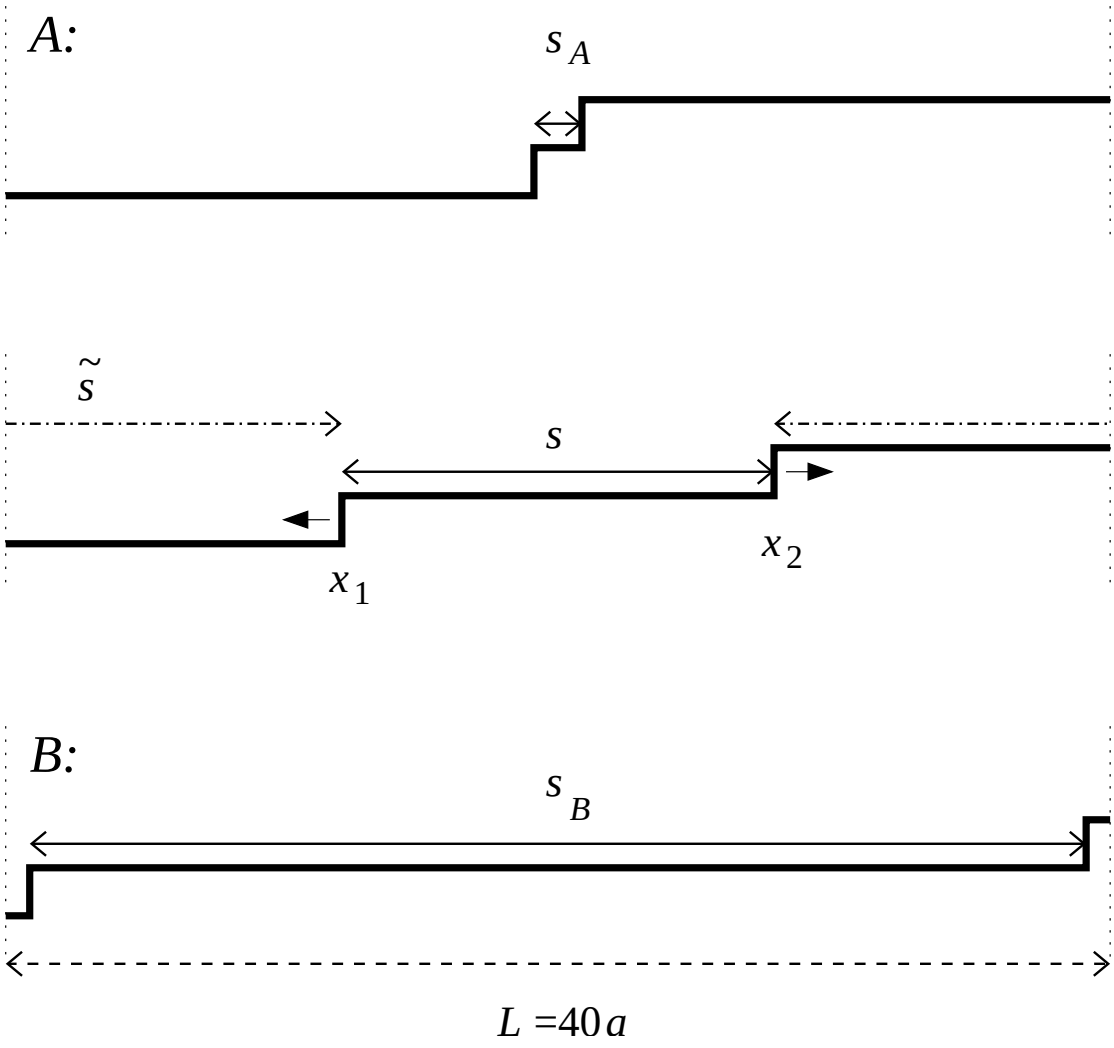

FIG. 9: Geometry used for calculating two-step interaction energy. Left and right boundaries are skew-periodic. Steps are moved from configuration A to configuration B in such a way that the total area under the curve remains constant (mass is conserved).

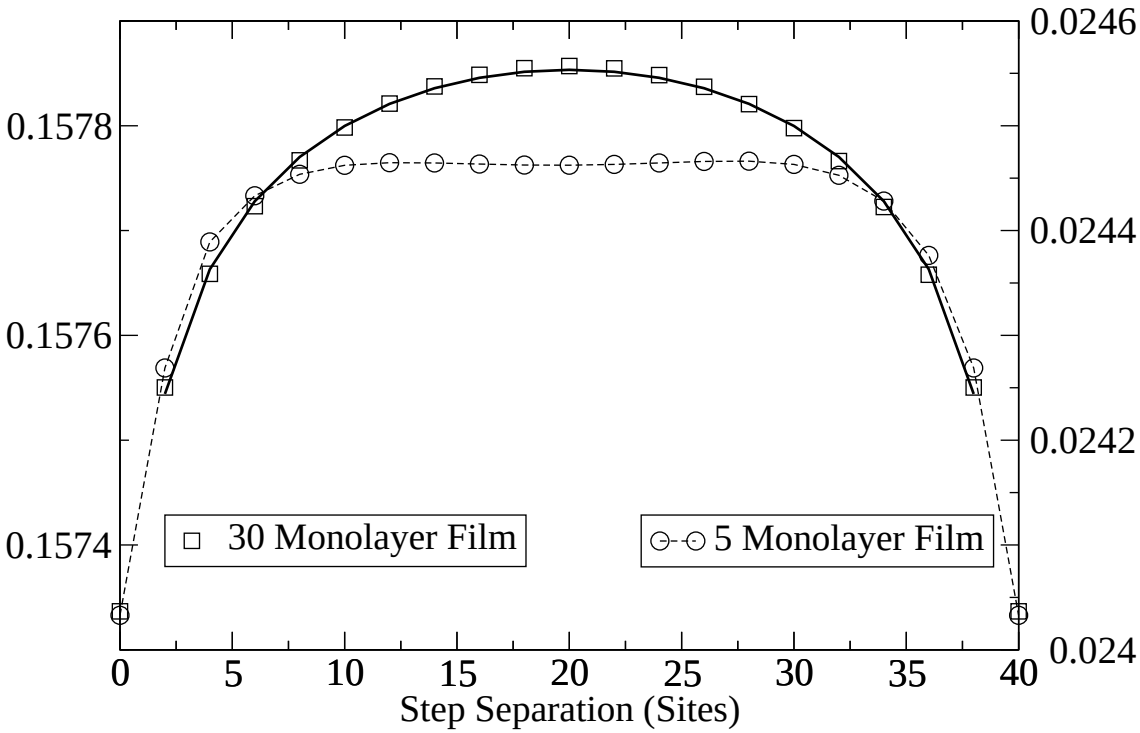

FIG. 10: Total system energy for a step moving from configuration A ($s = 0$) to configuration B ($s = 20$), for both a 30 atom thick epilayer (squares, left axis) and a 5 atom thick epilayer (circles, right axis). Both calculations are on a 30-layer substrate. Solid line is logarithmic fit.

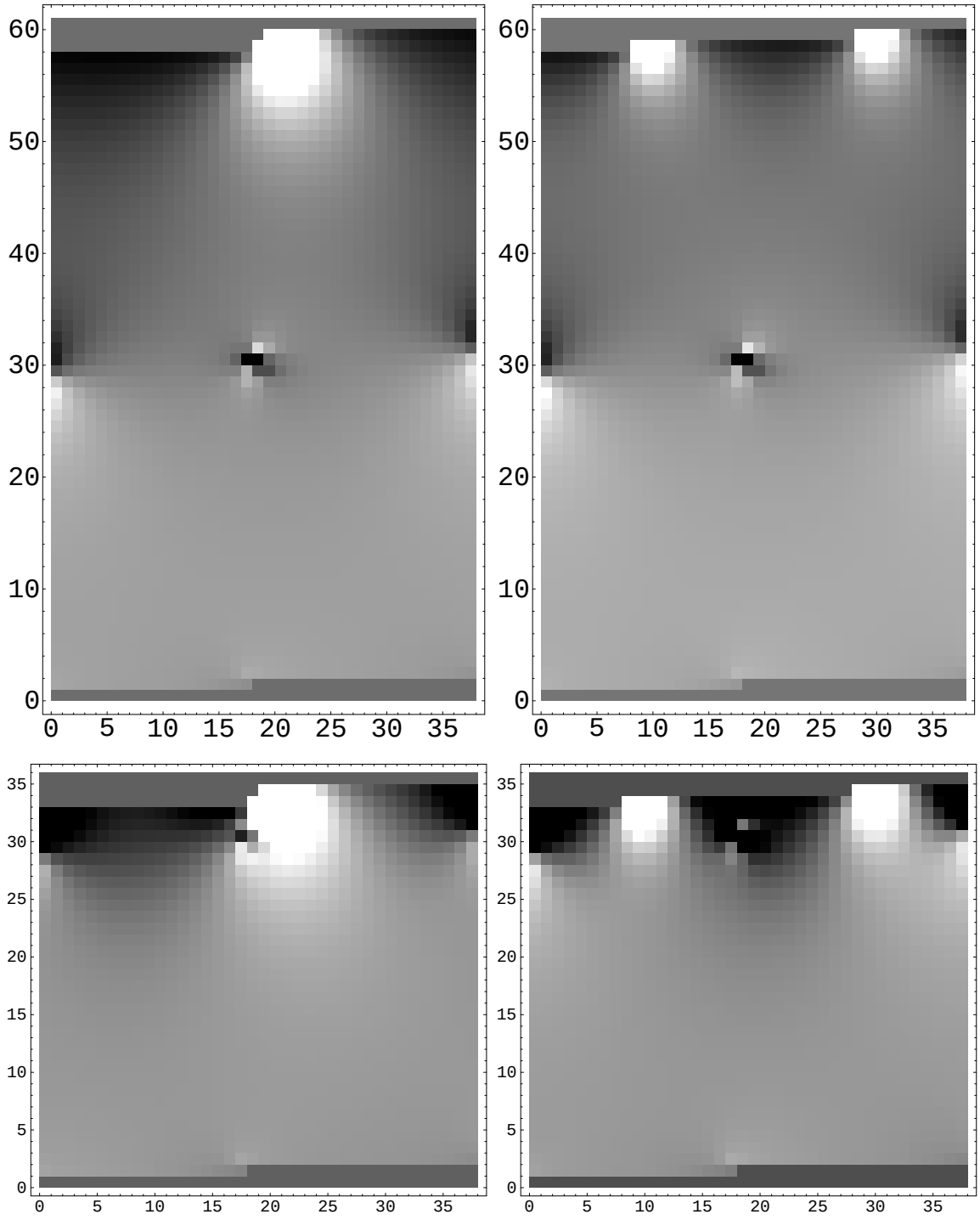

FIG. 11: Hydrostatic strain for sample configurations from the Figure 10 calculation. The left column is for $s = 0$ and the right is for $s = L/2 = 20$. The top row is a 30-monolayer film and the bottom row is a 5-monolayer film.